Journal of Math-for-Industry, Vol. 3 (2011C-7), pp. 53–60

Math-for-industry
Education & Research Hub

Numerical simulation of multicomponent compressible flow in porous medium

Ondřej Polívka and Jiří Mikyška

Revised on October 25, 2011

Abstract. The paper deals with the numerical modeling of compressible single-phase flow of a mixture composed of several components in a porous medium. The mathematical model is formulated by means of Darcy's law, components continuity equations, constitutive relations, and appropriate initial and boundary conditions. The problem is solved numerically using a combination of the mixed-hybrid finite element method for Darcy's law discretization and the finite volume method for the discretization of the transport equations. This approach provides exact local mass balance. The time discretization is carried out by the Euler method. The resulting large system of nonlinear algebraic equations is solved by the Newton-Raphson iterative method. The dimensions of obtained system of linear algebraic equations are significantly reduced so that they do not depend on the number of mixture components. The convergence of the numerical scheme is verified on two problems of methane injection into a homogeneous 2D reservoir filled with propane which is horizontally or vertically oriented.

Keywords. Mixed-hybrid finite element method, finite volume method, Newton-Raphson method, single-phase compressible multicomponent flow, miscible displacement

1. Introduction

The reliable prediction of transport of multicomponent mixtures in the subsurface is important for many applications including oil recovery or CO_2 sequestration. The traditional approaches use either the fully implicit (fully coupled) method or a sequential method [20, 5]. The fully implicit method is stable, allows for long time steps, but leads to extremely large systems of linear algebraic equations whose size is proportional to the number of components. Alternatively, one can use sequential solution procedures like IMPEC (implicit pressure, explicit concentrations) [13]. In this approach, a pressure equation is formulated by summing up the transport equations [20, 5] or by other method [12, 21, 1]. The pressure equation is solved implicitly using the concentrations from the previous time step. Next, the mole fractions are updated using explicit methods. This procedure allows to reduce the size of the solved system as only pressure is solved implicitly. However, this approach is conditionally stable and the time step has to be chosen prohibitively small in many cases.

In this paper, we deal with the numerical modeling of the compressible single-phase flow of a mixture composed of several components in a porous medium which is suitable for description of multicomponent subsurface transport. We propose a new approach based on a combination of the mixed-hybrid finite element method (MHFEM) and the finite volume method (FVM). Similarly to the implicit schemes, our method leads to large systems of linear algebraic equations, but it is possible to reduce the size of the final system of equations to a size independent on the number of mixture components. Therefore, the solution cost is comparable with the traditional sequential approaches. Unlike in other sequential approaches, no pressure equation has to be formed as pressure is evaluated directly from the equation of state.

The paper is structured as follows. First, we present the mathematical model of the problem. Then, the numerical methods used for derivation of the computational scheme are described together with the proposed computational algorithm. Finally, we present computed numerical results verifying convergence of the numerical scheme.

2. Mathematical model

Let $\Omega \subset \mathbb{R}^2$ be a bounded domain with porosity ϕ [-], and $(0,\tau)$ be the time interval [s]. Consider the single-phase compressible flow of a fluid with N_C components in the domain at a constant temperature T [K]. Neglecting diffusion, the transport of the components is described by the following molar balance equations [12]

$$\frac{\partial(\phi c_i)}{\partial t} + \nabla \cdot (c_i \mathbf{q}) = f_i\,, \quad i = 1, \ldots, N_C\,, \qquad (1)$$
$$c_i = c_i(\mathbf{x}, t)\,, \quad \mathbf{x} \in \Omega\,,\ t \in (0,\tau)\,,$$

where unknown quantities c_i, $i = 1, \ldots, N_C$, are the molar concentrations of the components [$\mathrm{mol\,m^{-3}}$]. On the

right hand side of equation (1), f_i [mol m^{-3}s^{-1}] denotes the sink/source term. Darcy's velocity $\mathbf{q}$ [m s^{-1}] is given by Darcy's law (see [2])

$$\mathbf{q} = -\mu^{-1}\mathbf{K}(\nabla p - \varrho\mathbf{g}) , \tag{2}$$

where $\mathbf{K} \in [L^\infty(\Omega)]^{2\times 2}$ is the medium intrinsic permeability [m^2] (generally symmetric and uniformly positive-definite tensor satisfying (B.7)), μ is the viscosity [kg m^{-1}s^{-1}], ∇p denotes a gradient of the pressure p [Pa], $\mathbf{g}$ is the gravitational acceleration vector [m s^{-2}], and ϱ is the fluid density [kg m^{-3}]. Equations (1) and (2) are coupled with constitutive relations expressing dependencies

$$\begin{gathered} p = p\,(c_1, \ldots, c_{N_C}, T)\ , \quad \mu = \mu\,(c_1, \ldots, c_{N_C}, T)\ , \\ \varrho = \varrho\,(c_1, \ldots, c_{N_C})\ . \end{gathered} \tag{3}$$

In this work, pressure is prescribed by the Peng-Robinson equation of state (PR EOS), while viscosity is given by the Lohrenz-Bray-Clark (LBC) method. Details of relations (3) are presented in Appendix A.

The initial and boundary conditions are given by

$$c_i(\mathbf{x}, 0) = c_i^0(\mathbf{x})\,, \qquad \mathbf{x} \in \Omega\,,\ i = 1, \ldots, N_C\,, \tag{4a}$$

$$c_i(\mathbf{x}, t) = c_i^D(\mathbf{x}, t)\,, \quad \mathbf{x} \in \Gamma_c(t)\,,\ t \in (0, \tau)\,,\ i = 1, \ldots, N_C\,, \tag{4b}$$

$$p(\mathbf{x}, t) = p^D(\mathbf{x}, t)\,, \quad \mathbf{x} \in \Gamma_p\,,\ t \in (0, \tau)\ , \tag{4c}$$

$$\mathbf{q}(\mathbf{x}, t) \cdot \mathbf{n}(\mathbf{x}) = q^N(\mathbf{x}, t)\,, \quad \mathbf{x} \in \Gamma_q\,,\ t \in (0, \tau)\ , \tag{4d}$$

where $\mathbf{n}$ is the unit outward normal vector to the boundary $\partial\Omega$. Equations (4c) and (4d) determine the Dirichlet and Neumann boundary conditions on the Γ_p, Γ_q parts of the boundary, respectively, whereas conditions $\Gamma_p \cup \Gamma_q = \partial\Omega$ and $\Gamma_p \cap \Gamma_q = \emptyset$ must be satisfied. The boundary condition (4b) for molar concentration is also the Dirichlet type. The set $\Gamma_c(t)$ denotes the inflow part of the boundary $\partial\Omega$ in time t, i.e.

$$\Gamma_c(t) = \{\mathbf{x} \in \partial\Omega \,|\, \mathbf{q}(\mathbf{x}, t) \cdot \mathbf{n}(\mathbf{x}) < 0\}\ .$$

3. Numerical solution

The system of equations (1)–(4) is solved numerically by a combination of the mixed-hybrid finite element method (MHFEM), for Darcy's law (2), and the finite volume method (FVM), for transport equations (1). The subsequent scheme is derived using the Euler method for time discretization and linearized by the Newton-Raphson method (NRM).

We consider a 2D polygonal domain Ω with the boundary $\partial\Omega$ which is covered by a spatial triangulation $\mathcal{T}_\Omega$ consisting of triangles or quadrilaterals. Let us denote K the element of the mesh $\mathcal{T}_\Omega$ with area $|K|$, E the edge of an element with the length $|E|$, N_K the number of elements of the triangulation, and N_E the number of edges of the mesh.

3.1. Discretization of Darcy's law

Darcy's velocity $\mathbf{q}$ can be approximated in the Raviart-Thomas space of the lowest order (RT^0_K) over the element $K \in \mathcal{T}_\Omega$ as

$$\mathbf{q} = \sum_{E \in \partial K} q_{K,E}\mathbf{w}_{K,E}\,, \tag{5}$$

where the coefficient $q_{K,E}$ is the flux of vector function $\mathbf{q}$ through the edge E of the element K with respect to outer normal, and $\mathbf{w}_{K,E}$ represents the piecewise linear RT^0_K–basis function associated with the edge E (see [3, 4, 17] or Appendix B).

By expressing the pressure gradient from Darcy's law (2), we obtain

$$\nabla p = -\mu\mathbf{K}^{-1}\mathbf{q} + \varrho\mathbf{g}\,. \tag{6}$$

Multiplying (6) by the basis function $\mathbf{w}_{K,E}$, integrating over K, taking advantages of the RT^0_K space (see Appendix B), and using (5) on the right side and the Green theorem on the left side together with the mean value theorem, we derive a discrete form of Darcy's law

$$q_{K,E} = \mu_K^{-1}\left(\alpha_E^K p_K - \sum_{E' \in \partial K} \beta_{E,E'}^K p_{K,E'} + \gamma_E^K \varrho_K\right)\,, \tag{7}$$

for $E \in \partial K$. In equation (7), $\alpha_E^K, \beta_{E,E'}^K$, and γ_E^K are coefficients dependent on the mesh geometry and on the local values of permeability (details in Appendix B); p_K is the cell pressure average; $p_{K,E'}$ is the edge pressure average; and μ_K, ϱ_K denote the mean values of viscosity and density over the cell K, respectively.

The continuity of flux and pressure on the edge E between neighboring elements $K, K' \in \mathcal{T}_\Omega$ can be written as

$$q_{K,E} + q_{K',E} = 0\,, \tag{8}$$

$$p_{K,E} = p_{K',E} =: p_E\,. \tag{9}$$

Boundary conditions (4c), (4d) expressed in a discrete form read as

$$p_{K,E} = p^D(E)\,, \quad \forall E \subset \Gamma_p\,, \tag{10a}$$

$$q_{K,E} = q^N(E)\,, \quad \forall E \subset \Gamma_q\,, \tag{10b}$$

where $p^D(E)$ is the prescribed value of the pressure p averaged on the edge E, and $q^N(E)$ is prescribed flux through the edge E.

The flux can be eliminated by substituting $q_{K,E}$ from (7) into equations (8) and (10b). For further derivation, let us consider time dependent quantities at time t_{n+1} denoted by upper index $n+1$. Then, equations (7)–(10) transform to the following system of N_E linear algebraic equations

$$F_E \equiv \begin{cases} \displaystyle\sum_{K:E\in\partial K} \left(\mu_K^{n+1}\right)^{-1}\Bigg(\alpha_E^K p_K^{n+1} - \sum_{E'\in\partial K} \beta_{E,E'}^K p_{K,E'}^{n+1} \\ \qquad + \gamma_E^K \varrho_K^{n+1}\Bigg) = 0\,, \quad \forall E \not\subset \partial\Omega\,, \\ \left(\mu_K^{n+1}\right)^{-1}\Bigg(\alpha_E^K p_K^{n+1} - \displaystyle\sum_{E'\in\partial K} \beta_{E,E'}^K p_{K,E'}^{n+1} \\ \qquad + \gamma_E^K \varrho_K^{n+1}\Bigg) - q^N(E) = 0\,, \quad \forall E \subset \Gamma_q\ , \\ p_{K,E}^{n+1} - p^D(E) = 0\,, \quad \forall E \subset \Gamma_p\ . \end{cases} \tag{11}$$

Herein, the symbol $\sum_{K:E\in\partial K}$ denotes the sum over the elements containing edge E. A similar procedure leading to the mixed-hybrid formulation can be found in [16].

3.2. Approximation of the transport equations

Transport equations (1) with the initial and boundary conditions (4) are discretized using the FVM [14]. Integrating (1) over an arbitrary element K from the mesh $\mathcal{T}_\Omega$, and using the Green theorem, we obtain

$$\frac{\mathrm{d}}{\mathrm{d}t}\int_K \phi(\mathbf{x})c_i(\mathbf{x},t) + \int_{\partial K} c_i(\mathbf{x},t)\mathbf{q}(\mathbf{x},t)\cdot\mathbf{n}_{\partial K}(\mathbf{x}) = \int_K f_i(\mathbf{x}),\quad i=1,\dots,N_C. \tag{12}$$

By applying the mean value theorem, and denoting $\phi_K, c_i|_K, f_i|_K$ the averaged values of ϕ, c_i, f_i $(i=1,\dots,N_C)$, respectively, over the cell K, we derive from (12)

$$\frac{\mathrm{d}(\phi_K c_i|_K)}{\mathrm{d}t}|K| + \sum_{E\in\partial K} \widetilde{c_i}|_E \underbrace{\int_E \mathbf{q}\cdot\mathbf{n}_{K,E}}_{=q_{K,E}} = f_i|_K|K|, \tag{13}$$

where $\widetilde{c_i}|_E$ denotes the concentration c_i on the edge E. The integral in (13) is equal to the flux through the edge E from element K (the component of $\mathbf{q}$ in the direction of outward normal to E).

Let us suppose that the porosity does not depend on time. The time derivative of $c_i|_K$ in (13) is approximated by the time difference with a time step Δt_n. Using the Euler method (see [14]), we obtain for every n, all elements $K\in\mathcal{T}_\Omega$, and components $i=1,\dots,N_C$

$$F_{K,i} \equiv \phi_K|K|\frac{c_i|_K^{n+1}-c_i|_K^n}{\Delta t_n} + \sum_{E\in\partial K}\widetilde{c_i}|_E^n\, q_{K,E}^{n+1}\left(p_{K,E}^{n+1}, c_1|_K^{n+1},\dots,c_{N_C}|_K^{n+1}\right) - f_i|_K|K| = 0, \tag{14}$$

where $q_{K,E}^{n+1}$ is given by (7). The value of $\widetilde{c_i}|_E^n$ is chosen from neighboring element in the upwind direction, i.e.

$$\widetilde{c_i}|_E^n = \begin{cases} c_i|_K^n & \text{for} \quad q_{K,E}^{n+1}\geq 0,\\ c_i|_{K'}^n & \text{for} \quad q_{K,E}^{n+1}<0 \ \wedge E\notin\partial\Omega : K\cap K' = E,\\ c_i^D|_E^n & \text{for} \quad q_{K,E}^{n+1}<0 \ \wedge E\subset\partial\Omega, \end{cases} \tag{15}$$

where c_i^D represents the concentration of the i-th component on the inflow boundary. Note that the scheme is almost fully implicit – the only term in (14) which is evaluated explicitly is the value of $\widetilde{c_i}|_E^n$.

The initial and boundary conditions (4a) and (4b) are approximated as

$$c_i|_K^0 = c_i^0(K), \qquad \forall K\in\mathcal{T}_\Omega,\ i=1,\dots,N_C, \tag{16a}$$

$$\widetilde{c_i}|_E^n = c_i^D(E,t_n), \quad \forall E\subset\Gamma_c(t),\ i=1,\dots,N_C,\ t_n<\tau. \tag{16b}$$

3.3. Combining the MHFEM and the FVM schemes

Let us use the notation F_E and $F_{K,i}$, for edge $E\in\{1,\dots,N_E\}$, element $K\in\{1,\dots,N_K\}$, and component $i\in\{1,\dots,N_C\}$, the left hand sides of equations (11) and (14) with $q_{K,E}^{n+1}$ substituted from relation (7). The cell averaged values $p_K = p_K(c_1|_K,\dots,c_{N_C}|_K)$, $\varrho_K = \varrho_K(c_1|_K,\dots,c_{N_C}|_K)$, and $\mu_K = \mu_K(c_1|_K,\dots,c_{N_C}|_K)$ are evaluated using constitutive relations (3). The system of $N_E + N_K\times N_C$ equations

$$\mathbf{F} = [F_1,\dots,F_{N_E};\ F_{1,1},\dots,F_{1,N_C},\dots,F_{N_K,1},\dots,F_{N_K,N_C}]^T = \mathbf{0}$$

for unknown molar concentrations $c_1|_K^{n+1},\dots,c_{N_C}|_K^{n+1}$, $K\in\{1,\dots,N_K\}$, and edge averaged pressures p_E^{n+1}, $E\in\{1,\dots,N_E\}$, is a nonlinear system of algebraic equations which we solve using the NRM. The resulting system of linear algebraic equations is shown in Fig. 1, where the sparse Jacobi matrix is unsymmetric, and the unknown vector is represented by corrections of molar concentrations and edge pressures. The nonzero black-coloured values in Fig. 1 are given by partial derivatives

$$(\mathbf{J}_K)_{i,j} = \frac{\partial F_{K,i}}{\partial c_j|_K^{n+1}}, \qquad (\mathbf{J}_{K,E})_i = \frac{\partial F_{K,i}}{\partial p_{K,E}^{n+1}}, \tag{17}$$

$$(\mathbf{J}_{E,K})_j = \frac{\partial F_E}{\partial c_j|_K^{n+1}}, \qquad J_{E,E'} = \frac{\partial F_E}{\partial p_{K,E'}^{n+1}}, \tag{18}$$

where $J_{E,E'}$ is element of the matrix $\mathbf{J}_{E,E'}$ and $i,j = 1,\dots,N_C$; $K=1,\dots,N_K$; $E,E'=1,\dots,N_E$. The partial derivatives in (17) can be evaluated analytically using (3), (11), and (14).

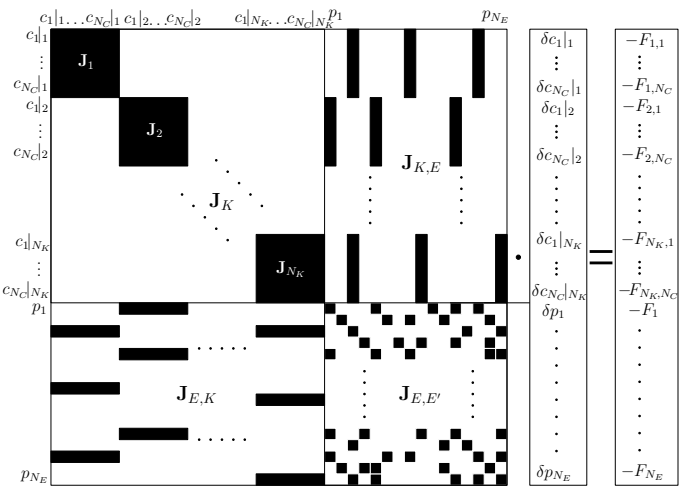

Figure 1: Structure of the system of linear algebraic equations in the NRM.

The size of the system in Fig. 1 can be reduced by inverting the $\mathbf{J}_K$ blocks for all K (the inversion is possible since the blocks are diagonally dominant for small time steps) and eliminating vectors $\mathbf{J}_{E,K}$ for all E,K. Then, we derive

a system of N_E equations for N_E corrections of pressures p_E

$$\sum_{K:E\in\partial K}\sum_{E'\in\partial K}\left(J_{E,E'}-\mathbf{J}_{E,K}\mathbf{J}_K^{-1}\mathbf{J}_{K,E'}\right)\delta p_{E'} = \sum_{K:E\in\partial K}\mathbf{J}_{E,K}\mathbf{J}_K^{-1}\mathbf{F}|_K - F_E\,, \quad (19)$$

where $E=1,\dots,N_E$, $\mathbf{F}|_K=[F_{K,1},\dots,F_{K,N_C}]^T$. Once δp_E are computed, corrections of concentrations $\Delta\mathbf{c}|_K=[\delta c_1|_K,\dots,\delta c_{N_C}|_K]^T$ on each cell K can be evaluated by solving

$$\Delta\mathbf{c}|_K=-\mathbf{J}_K^{-1}\left(\mathbf{F}|_K+\sum_{E'\in\partial K}\delta p_{E'}\,\mathbf{J}_{K,E'}\right), \quad (20)$$

for $K=1,\dots,N_K$. The corrections δp_E and $\delta c_i|_K$ for all edges, components, and elements obtained in an iteration of the NRM are added to the values p_E^{n+1} and $c_i|_K^{n+1}$ from the previous iteration. The iteration process stops if the condition

$$\left\|[\delta c_1|_1,\dots,\delta c_{N_C}|_{N_K},\delta p_1,\dots,\delta p_{N_E}]^T\right\|<\varepsilon \quad (21)$$

is satisfied for a chosen $\varepsilon>0$ (see [19]).

4. Computational algorithm

Numerical solution can be computed in the following steps:

1. Initialize geometry, physical and chemical parameters, and molar concentrations from initial condition; generate a domain triangulation.
2. Calculate pressures p_K on each element using the PR EOS from initial molar concentrations, then evaluate all edge pressures p_E by averaging p_K on neighboring elements.
3. Repeat until the predetermined final time is reached ($t_n<\tau$):
   (a) Repeat the NRM iterations until a convergence criterion is satisfied:
      i. Compute viscosities μ_K^{n+1} on each cell using the LBC method (A.7).
      ii. Compute densities ϱ_K^{n+1} on each cell using (A.3).
      iii. Calculate pressures p_K^{n+1} on each element using the PR EOS (A.1).
      iv. Assemble and solve the system (19) for edge pressure corrections δp_E.
      v. Calculate molar concentration corrections $\delta c_i|_K$ for each component and each element from (20).
      vi. Add the corrections δp_E and $\delta c_i|_K$ to p_E^{n+1} and $c_i|_K^{n+1}$, respectively, check the convergence (21).
   (b) Continue to the next time level ($n\to n+1$).

In steps i.–iii. μ_K^{n+1}, ϱ_K^{n+1}, and p_K^{n+1} are computed using the data from the last available Newton iteration. In the first iteration, data from the previous time step are used.

5. Numerical results

Let us consider a 2D square domain $50\times50\,\mathrm{m}^2$ which represents a cut of a propane reservoir with porosity $\phi=0.2$ and isotropic permeability $\mathbf{K}=k=10^{-14}\,\mathrm{m}^2$ at initial pressure $p=5\cdot10^6\,\mathrm{Pa}$ and temperature $T=397\,\mathrm{K}$ in a horizontal or vertical position. In the left bottom corner of the reservoir, methane is injected and in the right top corner, the mixture of methane and propane is produced (Fig. 2). The injection rate $f_1|_K$ is $2.643\cdot10^{-2}/|K|\ \mathrm{mol\,m^{-3}s^{-1}}$, where $|K|$ is the area of the corner grid element. Physical-chemical properties of the mixture are summarized in Table 1. In all examples the initial data are chosen so that the mixture stays in the single-phase state. The boundary of the domain is impermeable except the outflow corner, where pressure $p=5\cdot10^6\,\mathrm{Pa}$ is maintained. The computational grid with $2\times m\times m$ elements is shown in Fig. 2 (where $m=10$). Parameter ε from the NRM convergence criterion (21) was chosen 10^{-6} for all computations. The system of equations (19) was solved using UMFPACK [6, 7, 8, 9].

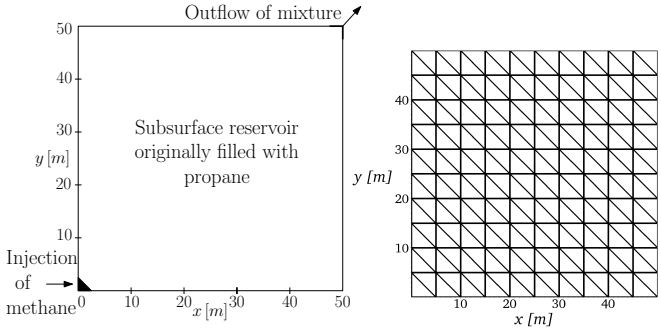

Figure 2: A scheme of simulated reservoir and a structure of the computational grid.

i (component)	p_{ci} [Pa]	T_{ci} [K]
1 (CH_4)	$4.58373\cdot10^6$	$1.89743\cdot10^2$
2 (C_3H_8)	$4.248\cdot10^6$	$3.6983\cdot10^2$

i (component)	V_{ci} [$\mathrm{m^3mol^{-1}}$]	M_i [$\mathrm{kg\,mol^{-1}}$]
1 (CH_4)	$9.897054\cdot10^{-5}$	$1.62077\cdot10^{-2}$
2 (C_3H_8)	$2.000001\cdot10^{-4}$	$4.40962\cdot10^{-2}$

i (component)	ω_i [-]	δ_{i1} [-]	δ_{i2} [-]
1 (CH_4)	$1.14272\cdot10^{-2}$	0	0.0365
2 (C_3H_8)	$1.53\cdot10^{-1}$	0.0365	0

Table 1: Relevant parameters of the PR EOS (see Appendix A) for methane CH_4 and propane C_3H_8. Volume translation is not used.

5.1. Convergence analysis in horizontal case

We will test convergence of the numerical scheme, derived in section 3, using a pseudoanalytical solution – the numerical solution computed on the finest grid $m=160$

(2×160×160 grid cells). Experimental order of convergence (EOC) will be computed between grids $m = 10$, $m = 20$, and $m = 40$ using the L^1, L^2, and L^∞ consistent norms for errors E_m in comparison with the solution on the grid $m = 160$. The error is computed on the finest grid by projecting the solutions from the coarser grids to the finest grid and using the linear interpolation. The time step for the solution $m = 160$ is chosen constant $\Delta t = 750\,\mathrm{s}$. For the solutions on coarser grids, Δt is 4 times larger with each mesh refinement ($\Delta t \sim m^{-2}$), i.e. $\Delta t = 12000\,\mathrm{s}$ for $m = 40$, $\Delta t = 48000\,\mathrm{s}$ for $m = 20$, and $\Delta t = 192000\,\mathrm{s}$ for $m = 10$. The EOC in a norm $\|.\|_\nu$ is given by

$$\mathrm{EOC}_\nu = \frac{\ln \|E_{m_1}\|_\nu - \ln \|E_{m_2}\|_\nu}{\ln m_2 - \ln m_1},$$

where E_{m_1} and E_{m_2} are the numerical solution errors on the grids with parameters m_1 and m_2, respectively.

The convergence analysis is, at first, performed on a problem of injection of methane into a horizontal propane reservoir (i.e. no gravity is considered). The EOC and errors for the situation at time $\tau = 6 \cdot 10^6\,\mathrm{s}$ are included in Table 2. The next Table 3 contains the data from time $\tau = 2.4 \cdot 10^7\,\mathrm{s}$, and a comparison of the solutions on the individual grids at this time is depicted in Fig. 3.

Grid (m)	$\|E_m\|_1$	EOC_1	$\|E_m\|_2$	EOC_2
10	$1.1025 \cdot 10^5$		$6.5336 \cdot 10^3$	
		0.6223		0.5086
20	$7.1621 \cdot 10^4$		$4.5922 \cdot 10^3$	
		0.8179		0.6814
40	$4.0627 \cdot 10^4$		$2.8635 \cdot 10^3$	

Grid (m)	$\|E_m\|_\infty$	EOC_∞
10	$1.1204 \cdot 10^3$	
		0.5077
20	$7.8804 \cdot 10^2$	
		0.5298
40	$5.4584 \cdot 10^2$	

Table 2: Experimental orders of convergence and errors of methane concentration c_1, $g = 0$, at time $\tau = 6 \cdot 10^6\,\mathrm{s}$ compared with the numerical solution on the grid $m = 160$ ($2 \times m \times m$ elements) and time step $\Delta t = 750\,\mathrm{s}$. On coarser grids, $\Delta t \sim m^{-2}$.

Grid (m)	$\|E_m\|_1$	EOC_1	$\|E_m\|_2$	EOC_2
10	$3.4079 \cdot 10^5$		$1.109 \cdot 10^4$	
		0.6514		0.5273
20	$2.1697 \cdot 10^5$		$7.6948 \cdot 10^3$	
		0.833		0.6814
40	$1.218 \cdot 10^5$		$4.7982 \cdot 10^3$	

Grid (m)	$\|E_m\|_\infty$	EOC_∞
10	$1.0485 \cdot 10^3$	
		0.584
20	$6.9948 \cdot 10^2$	
		0.4748
40	$5.0333 \cdot 10^2$	

Table 3: Experimental orders of convergence and errors of methane concentration c_1, $g = 0$, at time $\tau = 2.4 \cdot 10^7\,\mathrm{s}$ compared with the numerical solution on the grid $m = 160$ ($2 \times m \times m$ elements) and time step $\Delta t = 750\,\mathrm{s}$. On coarser grids, $\Delta t \sim m^{-2}$.

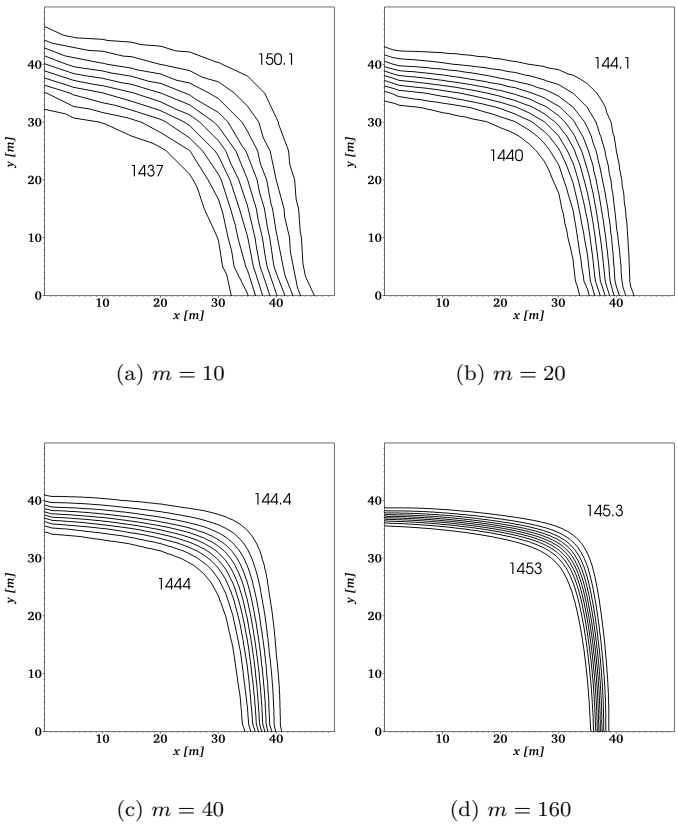

(a) $m = 10$ (b) $m = 20$

(c) $m = 40$ (d) $m = 160$

Figure 3: Contours of methane concentration c_1 at $\tau = 2.4 \cdot 10^7\,\mathrm{s}$ on different grids for Table 3. Isolines are distributed uniformly between the two displayed values.

5.2. Convergence analysis in vertical case

Similarly as in the previous part, we perform the convergence analysis on the problem of methane injection into a vertically oriented 2D propane reservoir. We use the same domain with boundary and data set as in the previous case, but this time, gravity effect is assumed ($g = 9.81\,\mathrm{m\,s^{-2}}$). Pressure $5 \cdot 10^6\,\mathrm{Pa}$ is fixed in the right upper corner of the domain. We present the errors in L^1 and L^2 norm. In Table 4, the EOC and errors from time $\tau = 6 \cdot 10^6\,\mathrm{s}$ are shown. Isolines of methane molar concentration are depicted in Fig. 4 on all computational grids. The last Table 5 contains the data from time $\tau = 2.4 \cdot 10^7\,\mathrm{s}$. As we can see, the EOC is lower in the case of the vertical domain with gravity than in the previous case of horizontal domain without gravity (cf. Tables 2 and 3).

Grid (m)	$\|E_m\|_1$	EOC_1	$\|E_m\|_2$	EOC_2
10	$1.3433 \cdot 10^5$		$8.644 \cdot 10^3$	
		0.5973		0.4441
20	$8.8787 \cdot 10^4$		$6.3535 \cdot 10^3$	
		0.7717		0.59
40	$5.2006 \cdot 10^4$		$4.2211 \cdot 10^3$	

Table 4: Experimental orders of convergence and errors of methane concentration c_1, $g = 9.81\,\mathrm{m\,s^{-2}}$, at time $\tau = 6 \cdot 10^6\,\mathrm{s}$ compared with the numerical solution on the grid $m = 160$ ($2 \times m \times m$ elements) and time step $\Delta t = 750\,\mathrm{s}$. On coarser grids, $\Delta t \sim m^{-2}$.

Grid (m)	$\|E_m\|_1$	EOC_1	$\|E_m\|_2$	EOC_2
10	$6.5964 \cdot 10^5$		$2.2368 \cdot 10^4$	
20	$5.0932 \cdot 10^5$	0.3731	$1.8978 \cdot 10^4$	0.2371
40	$3.7703 \cdot 10^5$	0.4339	$1.5975 \cdot 10^4$	0.2485

Table 5: Experimental orders of convergence and errors of methane concentration c_1, $g = 9.81\,\mathrm{m\,s^{-2}}$, at time $\tau = 2.4 \cdot 10^7\,\mathrm{s}$ compared with the numerical solution on the grid $m = 160$ ($2 \times m \times m$ elements) and time step $\Delta t = 750\,\mathrm{s}$. On coarser grids, $\Delta t \sim m^{-2}$.

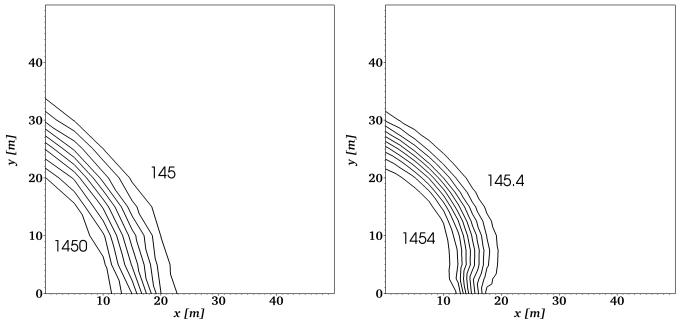

(a) $m = 10$ (b) $m = 20$

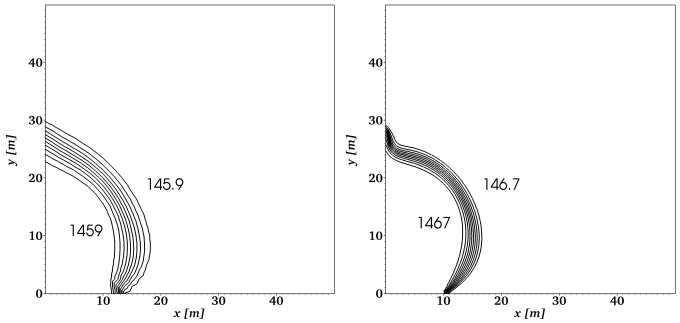

(c) $m = 40$ (d) $m = 160$

Figure 4: Contours of methane concentration c_1 at $\tau = 6 \cdot 10^6\,\mathrm{s}$ on different grids for Table 4. Isolines are distributed uniformly between the two displayed values.

CPU-times for the simulation of the horizontal and vertical domain on particular grids can be found in Table 6.

Grid (m)	$g = 0$: CPU-time [s]	$g \neq 0$: CPU-time [s]
10	35	30
20	207	218
40	1976	2378
80	73538	35633
160	436365	554308

Table 6: Computational times for solutions computed on different grids on Dual-Core AMD Opteron(tm) Processor 2216, 2400 MHz (single core used), cache size 1 MB, and total memory 8 GB.

6. Conclusion

In this work, we have developed a new numerical scheme based on a combination of the MHFEM and FVM for simulation of single-phase compressible multicomponent flow in a porous medium. Unlike in traditional approaches, we evaluate the pressure directly from the equation of state. The system of nonlinear algebraic equations obtained by combining the MHFEM, FVM, and using the Euler method is linearized by the Newton-Raphson method. The size of the resulting system of linear algebraic equations depends on the number of mixture components. Therefore, we proposed a technique reducing significantly the system into a size that is independent on the number of mixture components. Consequently, computational costs are comparable with traditional sequential approaches. Although we tested the numerical model for two components, the advantage of this approach is expected to be larger in the more components case. Our method provides exact local mass balance (up to the non-linear solver error) which is important for solving problems especially in a heterogeneous medium. Convergence of the numerical scheme was successfully verified by evaluating the experimental order of convergence on two problems of methane injection into a horizontal and vertical propane reservoir. In the future work, we would like to improve the current model using the high order methods and to test it on problems involving more than two components.

Appendix A

Peng-Robinson equation of state

In this work, pressure is given by the PR EOS [18, 10] as

$$p = \frac{RT \sum_{i=1}^{N_C} c_i}{1 - \sum_{i=1}^{N_C} b_i\, c_i} - \frac{\sum_{i=1}^{N_C} \sum_{j=1}^{N_C} a_{ij}\, c_i\, c_j}{1 + 2 \sum_{i=1}^{N_C} b_i\, c_i - \left(\sum_{i=1}^{N_C} b_i\, c_i \right)^2}. \quad \text{(A.1)}$$

In equation (A.1), $R = 8.314472\,\mathrm{JK^{-1}mol^{-1}}$ is the universal gas constant, T the temperature [K], and

$$a_{ij} = (1 - \delta_{ij}) \sqrt{a_i a_j}\,, \quad a_i = \frac{0.45724\, R^2\, T_{ci}^{\,2}}{p_{ci}}\, \alpha_i\,,$$
$$\alpha_i = \Big(1 + \big(0.37464 + 1.54226\,\omega_i - 0.26992\,\omega_i^2\big) \cdot$$
$$\cdot \Big(1 - \sqrt{T_{ri}}\Big)\Big)^2\,, \quad T_{ri} = \frac{T}{T_{ci}}\,, \quad b_i = \frac{0.07780\, R\, T_{ci}}{p_{ci}}\,, \quad \text{(A.2)}$$

where δ_{ij} is the binary interaction coefficient [-]; T_{ci}, p_{ci}, ω_i, T_{ri} are the critical temperature, critical pressure, acentric factor [-], reduced temperature [-], respectively – all corresponding to the i-th component.

Density computation

The density-molar concentrations relation, according to [11], reads as

$$\varrho = \sum_{i=1}^{N_C} M_i \, c_i \,, \tag{A.3}$$

where M_i is the molar weight of the i-th component $[\mathrm{kg\,mol^{-1}}]$.

Lohrenz-Bray-Clark model for viscosity

In the numerical computations, the model proposed by Lohrenz, Bray, and Clark [15] in 1964 is used for estimation of (dynamic) viscosity of hydrocarbon mixtures. At first, empirical formulas for the viscosity μ_i^0 of low-pressure pure component fluids are evaluated as follows

$$\mu_i^0 = \begin{cases} 34 \cdot 10^{-5} \, {T_{ri}}^{0.94} / \xi_i & \text{for } T_{ri} \leq 1.5 \,, \\ 17.78 \cdot 10^{-5} \left(4.58 \, T_{ri} - 1.67\right)^{5/8} / \xi_i & \text{for } T_{ri} > 1.5 \,, \end{cases} \tag{A.4}$$

where

$$T_{ri} = \frac{T}{T_{ci}} \,, \quad \xi_i = \frac{{T_{ci}}^{1/6}}{{M_i}^{1/2} \, {p_{ci}}^{2/3}} \,, \quad i = 1, \ldots, N_C \,. \tag{A.5}$$

Next, we express the low-pressure viscosity of a mixture of N_C components as

$$\mu^0 = \frac{\sum\limits_{i=1}^{N_C} z_i \, \mu_i^0 \, \sqrt{M_i}}{\sum\limits_{i=1}^{N_C} z_i \, \sqrt{M_i}} \,, \tag{A.6}$$

where $z_i = c_i / c$ is the mole fraction of the i-th component. The final viscosity μ of the multicomponent fluid for higher pressures is given by

$$\begin{aligned} \left[\left(\mu - \mu^0\right) \xi + 10^{-4}\right]^{1/4} &= 0.1023 + 0.023364 \, c_r + \\ &+ 0.058533 \, c_r^2 - 0.040758 \, c_r^3 + 0.0093324 \, c_r^4 \,. \end{aligned} \tag{A.7}$$

In equation (A.7), c_r is called the reduced molar density defined as

$$c_r = c \sum_{i=1}^{N_C} z_i \, V_{ci} \,, \tag{A.8}$$

where V_{ci} is the critical molar volume of the i-th component. The parameter ξ in (A.7) is computable according to

$$\xi = \frac{\left(\sum\limits_{i=1}^{N_C} z_i \, T_{ci}\right)^{1/6}}{\left(\sum\limits_{i=1}^{N_C} z_i \, M_i\right)^{1/2} \left(\sum\limits_{i=1}^{N_C} z_i \, p_{ci}\right)^{2/3}} \,. \tag{A.9}$$

In relations (A.4)–(A.9) the temperatures T and T_{ci} are in Kelvins, molar weights M_i in grams per mole, critical pressures p_{ci} in atmospheres ($1\,\mathrm{atm} = 101325\,\mathrm{Pa}$), critical molar volumes V_{ci} in litres per mole, molar densities c and c_i in moles per litre, and viscosity μ is in the units of centipoise $\left(1\,\mathrm{cP} = 10^{-3}\mathrm{kg\,m^{-1}\,s^{-1}}\right)$.

Appendix B

In this part, we describe details of derivation of discrete Darcy's law (7) using the Raviart-Thomas space. Raviart-Thomas space of the lowest order RT_K^0, over an element K from a triangulation $\mathcal{T}_\Omega$ (consisting of triangles) of the domain Ω, is generated by the basis functions

$$\mathbf{w}_{K,E}(\mathbf{x}) = \frac{1}{2|K|} \left(\mathbf{x} - \mathbf{N}_{K,E}\right) \,, \quad \forall \mathbf{x} \in K \,, \; E \in \partial K \,, \tag{B.1}$$

where $\mathbf{N}_{K,E} \in K$ is a node against edge E. The basis functions (B.1) satisfy the following properties

$$\nabla \cdot \mathbf{w}_{K,E}(\mathbf{x}) = \frac{1}{|K|} \,, \quad \mathbf{w}_{K,E}(\mathbf{x}) \cdot \mathbf{n}_{K,E'} = \frac{\delta_{E,E'}}{|E|} \,. \tag{B.2}$$

Multiplying (6) with the basis function $\mathbf{w}_{K,E}$, and integrating over element K, we can write

$$\begin{aligned} \int_K \nabla p \cdot \mathbf{w}_{K,E'} = -\mu_K \sum_{E \in \partial K} q_{K,E} \int_K \mathbf{K}^{-1} \mathbf{w}_{K,E} \cdot \mathbf{w}_{K,E'} + \\ + \varrho_K \int_K \mathbf{g} \cdot \mathbf{w}_{K,E'} \,, \end{aligned} \tag{B.3}$$

where we have used (5) and the mean value theorem. Using the Green theorem, the mean value theorem, and properties (B.2), we obtain

$$\begin{aligned} \int_K \nabla p \cdot \mathbf{w}_{K,E'} = \sum_{E \in \partial K} \int_E p \, \mathbf{w}_{K,E'} \cdot \mathbf{n}_{K,E} - \int_K p \nabla \cdot \mathbf{w}_{K,E'} = \\ = \underbrace{\frac{1}{|E'|} \int_{E'} p}_{p_{K,E'}} - \underbrace{\frac{1}{|K|} \int_K p}_{p_K} \,. \end{aligned} \tag{B.4}$$

Denoting

$$A_{K,E,E'} = \int_K \mathbf{K}^{-1} \mathbf{w}_{K,E} \cdot \mathbf{w}_{K,E'} \,, \quad G_{K,E'} = \int_K \mathbf{g} \cdot \mathbf{w}_{K,E'} \,, \tag{B.5}$$

we combine (B.3) and (B.4) into

$$\mu_K \sum_{E \in \partial K} q_{K,E} A_{K,E,E'} = p_K - p_{K,E'} + \varrho_K G_{K,E'} \,. \tag{B.6}$$

Because $\mathbf{K}$ is uniformly positive-definite (see [16]), i.e.

$$\exists \alpha_0 > 0 : \alpha_0 \sum_{i=1}^{2} \xi_i^2 \leq \sum_{i,j=1}^{2} \left[K(\mathbf{x})\right]_{i,j} \xi_i \, \xi_j \,, \; \forall \xi \in \mathbb{R}^2 \,, \tag{B.7}$$

for almost all $\mathbf{x} \in \Omega$, it is possible to invert the matrix $\mathbf{A}_K = \left(A_{K,E,E'}\right)_{E,E' \in \partial K}$. Multiplying (B.6) in a vector form by $\mathbf{A}_K^{-1}$, we obtain

$$q_{K,E} = \mu_K^{-1} \left(\alpha_E^K p_K - \sum_{E' \in \partial K} \beta_{E,E'}^K p_{K,E'} + \gamma_E^K \varrho_K \right) \,, \tag{B.8}$$

which is Darcy's law (7) with coefficients α_E^K , $\beta_{E,E'}^K$, and γ_E^K given by

$$\alpha_E^K = \sum_{E' \in \partial K} A^{-1}_{K,E,E'} , \quad \beta^K_{E,E'} = A^{-1}_{K,E,E'} , \\ \gamma_E^K = \sum_{E' \in \partial K} A^{-1}_{K,E,E'} G_{K,E'} , \tag{B.9}$$

where $A^{-1}_{K,E,E'}$ is the element of the inverse matrix $\mathbf{A}_K^{-1}$.

Acknowledgements

This research has been supported by the projects Development of Computational Models for Simulation of CO2 Sequestration, P105/11/1507 of the Czech Science Foundation, and Numerical Methods for Multiphase Flow and Transport in Subsurface Environmental Applications, Kontakt ME10009 of Czech Ministry of Education, Youth and Sports.

References

[1] Acs, G., Doleschall, S., Farkas, E.: General Purpose Compositional Model, *Society of Petroleum Engineers Journal*, Vol.: 25, Issue: 4 (1985) 543–553.

[2] Bear, J., Verruijt, A.: Modeling Groundwater Flow and Pollution (1987), D. Reidel Publishing Company, Dordrecht, Holland.

[3] Brezzi, F., Fortin, M.: Mixed and Hybrid Finite Element Methods (1991), Springer-Verlag, New York Inc.

[4] Chavent, G., Roberts, J. E.: A unified physical presentation of mixed, mixed-hybrid finite elements and standard finite difference approximations for the determination of velocities in waterflow problems, *Advances in Water Resources*, 14(6) (1991).

[5] Chen, Z., Huan, G., Ma, Y.: Computational Methods for Multiphase Flows in Porous Media (2006), SIAM, Philadelphia.

[6] Davis, T. A.: A column pre-ordering strategy for the unsymmetric-pattern multifrontal method, *ACM Transactions on Mathematical Software*, vol 30, no. 2 (2004), pp. 165–195.

[7] Davis, T. A.: Algorithm 832: UMFPACK, an unsymmetric-pattern multifrontal method, *ACM Transactions on Mathematical Software*, vol 30, no. 2 (2004), pp. 196–199.

[8] Davis, T. A. and Duff, I. S.: A combined unifrontal/multifrontal method for unsymmetric sparse matrices, *ACM Transactions on Mathematical Software*, vol. 25, no. 1 (1999), pp. 1–19.

[9] Davis, T. A. and Duff, I. S.: An unsymmetric-pattern multifrontal method for sparse LU factorization, *SIAM Journal on Matrix Analysis and Applications*, vol 18, no. 1 (1997), pp. 140–158.

[10] Firoozabadi, A.: Thermodynamics of Hydrocarbon Reservoirs (1998), McGraw-Hill, NY.

[11] Holzbecher, E. O.: Modeling Density-Driven Flow in Porous Media: Principles, Numerics, Software (1998), Springer-Verlag, Berlin.

[12] Hoteit, H., Firoozabadi, A.: Multicomponent Fluid Flow by Discontinuous Galerkin and Mixed Methods in Unfractured and Fractured Media, *Water Resources Research* (2005), 41, W11412, doi:10.1029/2005WR004339.

[13] Huyakorn, P. S., Pinder, G. F.: Computational Methods in Subsurface Flow (1983), Academic Press, Inc., New York.

[14] Leveque, R. J.: Finite Volume Methods for Hyperbolic Problems (2002), Cambridge University Press, Cambridge.

[15] Lohrenz, J., Bray, B. G., Clark, C. R.: Calculating Viscosities of Reservoir Fluids From Their Compositions, *Journal of Petroleum Technology* Oct. (1964) 1171–1176.

[16] Maryška, J., Rozložník M., Tůma M.: Mixed-hybrid finite element approximation of the potential fluid flow problem, *Journal of Computational and Applied Mathematics* 63 (1995), 383–392.

[17] Mikyška, J., Firoozabadi, A.: Implementation of higher-order methods for robust and efficient compositional simulation, *Journal of Computational Physics* 229 (2010) 2898–2913.

[18] Peng, D. Y., Robinson, D. B.: A New Two-Constant Equation of State, *Industrial and Engineering Chemistry: Fundamentals 15* (1976) 59–64.

[19] Quarteroni, A., Sacco, R., Saleri, F.: Numerical Mathematics (2000), Springer-Verlag, New York.

[20] Russel, T. F., Wheeler, M. F.: Finite Element and Finite Difference Methods for Continuous Flows in Porous Media in: *The Mathematics of Reservoir Simulation, Frontiers in Applied Mathematics* (1983) 35–106, SIAM, Philadelphia.

[21] Young, L. C., Stephenson, R. E.: A Generalized Compositional Approach for Reservoir Simulation, *Society of Petroleum Engineers Journal*, Vol.: 23, Issue: 5 (1983) 727–742.

Ondřej Polívka and Jiří Mikyška
Department of Mathematics, Faculty of Nuclear Sciences and Physical Engineering, Czech Technical University in Prague, Trojanova 13, 120 00 Praha 2, Czech Republic
E-mail: ondrej.polivka(at)fjfi.cvut.cz
jiri.mikyska(at)fjfi.cvut.cz